

Chapter 8

Design of Half-Ring MIMO Antenna to Reduce the Mutual Coupling



K. Vasu Babu and B. Anuradha

Abstract We propose a novel, dual-polarized MIMO radiator, which consists of half rings, and included in the ring a square shape at the top side and half circular shape at bottom side operating from 2 to 10 GHz with a microstrip feeding. The suppression of mutual coupling is obtained by maintaining the separation between the patches around $0.25 \lambda_0$. The half-ring MIMO antenna is resonating at dual band of frequencies at 7.24 and 8.16 GHz with impedance bandwidths of 430 and 230 MHz, has $|S_{11}| < -10$ dB in the MIMO range from 2.0 to 10.0 GHz and has a mutual coupling with $|S_{21}| < -20$ dB. The radiator has a low ECC (envelope correlation coefficient) with values equal to approximately less than 0.025, which will prove that the half-ring MIMO radiator shows better diversity performance. The half-ring MIMO radiator has improved the parameters of reflection coefficient, mutual coupling, realized gain, group delay and real/imaginary impedances.

Keywords Multiple input-multiple output · Realized gain · ECC · Group delay · Real/imaginary impedances

Abbreviation

ECC	envelope correlation coefficient
GD	group delay
MIMO	multiple input-multiple output
NGD	negative group delay
UWB	ultra-wide band antenna

K. V. Babu (✉)
Department of ECE, VVIT, Guntur, Andhra Pradesh, India

B. Anuradha
Department of ECE, Sri Venkateswara University, Tirupati, Andhra Pradesh, India

8.1 Introduction

The major challenge in the design of any multiple input-multiple output (MIMO) antenna is when the antenna elements are at close proximity, it produces a mutual coupling. A few isolation techniques like using split ring resonators reduced the isolation to 20 dB [1], and by using common mode suppression of ultra-wide band antenna (UWB)-MIMO radiator reduces the isolation to 15.5 dB [2] and maintains an ECC value of 0.04. To reduce the mutual coupling, the design structure Minkowski produced multi-band [3] characteristics having S_{21} of 42 dB. A compact antenna having an area $23 \times 39.5 \text{ mm}^2$ and polarization diversity array produced an isolation of 20 dB operated between 2.5 and 12 GHz [4] whose ECC value maintained at less than 0.55. In [5] a parasitic approach like a UWB-MIMO radiator used a carbon film black operated from 2.5 to 11 GHz with reflection coefficient (S_{21}) of 20 dB. A floating parasitic decoupling structure [6] with a size of 33×45.5 produced a UWB system whose isolation ≤ 20 dB is achieved. An extendable MIMO array antenna has a low ECC around 0.025 and its peak gain 4 dBi was observed [7]. A wide-band MIMO antenna with band rejection [8], tri-band MIMO for defence and radio astronomy applications [9] was observed. For the mobile terminal applications, a compact G-shaped design [10] having an area of $50 \times 82 \text{ mm}^2$, operating in the frequency ranges from 2.2 to 13.3 GHz with isolation of ≤ 15 dB and a maximum gain of 4.78 dBi is achieved. Finally, it is interesting to observe that the proposed half-ring design structure reduced the mutual coupling to 40 dB. By using the techniques of optimization procedure finalized the dimensions. Table 8.1 shows the comparison with previous designs.

8.2 Antenna Construction and Its Geometry

The proposed structure having dimensions $46 \times 35 \text{ mm}^2$ is designed with a thickness of 1.5 mm on FR-4 substrate. The loss tangent ($\tan \delta$) is 0.02 and relative permittivity (ϵ_r) of the substrate is 4.3. The half-ring MIMO system produces a dual-band

Table 8.1 Comparison with existing systems

Refs.	Size (mm^2)	S_{11} (dB)	S_{21} (dB)	Gain (dBi)	f_L - f_H (GHz)
Irene and Rajesh [1]	40.5×40.5	45	20	6	3.1-10.6
Liu and Tu [2]	44×44	39	15.5	3.8	2.9-10.8
Braaten et al. [4]	23×39.5	27	20	3.6	2.0-10.0
Chen et al. [5]	50×40	32	15	4.73	2.5-11
Koul et al. [7]	38×90	20	20	4	3.1-16
Kim et al. [8]	55×13.5	35	17.2	4.2	3.1-10.6
Toktas [10]	50×82	34	15	4.78	2.2-13.3
Proposed system	46×35	29.25	21.89	4.75	2.0-10.0
		12.85	40	5	2.0-10.0

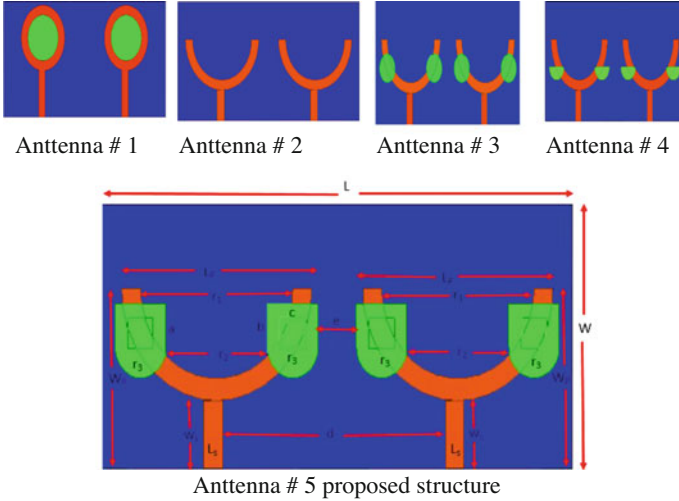


Fig. 8.1 Evolution stages of half-ring antenna

Table 8.2 Dimensions of half-ring MIMO antenna (in mm)

Parameter	L	W	L_p	W_p	r_1	r_2	r_3
Dimensions (mm)	50.5	35	38	25	3	10	2
Parameter	A	b	c	d	E	W_s	L_s
Dimensions (mm)	10	9	7	7	4	18	10

structure using the C-band applications. The step-by-step process of analysis is indicated in Fig. 8.1. Antenna # 1 shows that a strip is added to a circular ring which produced a reflection coefficient of 22 dB. Antenna # 2 represents the cutting of the half of the circles on both sides of total ring with S_{11} 13 dB. Antenna #3 represents adding half semi-circles on both sides of the patch and S_{11} is reached to 34 dB. Antenna #4 having a square patch is added to half circles on both sides to form a new structure whose S_{11} is 10 dB. Finally, Antenna #5 represents the proposed structure having the reflection coefficient greater than 25 dB and transmission coefficient of 40 dB. The design dimensions of the half-ring MIMO structure are listed in Table 8.2.

Finally, the designed structure having the dual band of operation produces the parameters S_{11} and S_{21} maintained less than 10 and 20 dB. In this design, strengthening the parameter mutual coupling between the two symmetrical radiators distance can be considered as 4 mm.

Figure 8.2 indicates the S -parameter evolution of each stage of half-ring MIMO design which shows all the cases $S_{11} \leq -10$ dB. Figure 8.3 shows the comparison of S parameters (S_{11} and S_{21}), which shows that a greater improvement in the mutual coupling observed at 7.2 GHz is 21.89 dB and at 8.1 GHz it almost touches to 40 dB reduction. Figure 8.4 shows the S_{21} comparison at different distances. This result shows that a greater interference between the patches is reduced. Figure 8.5 depicted

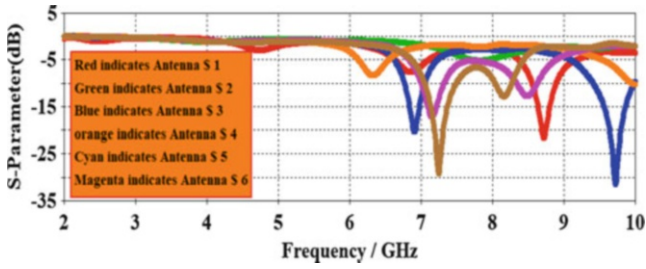


Fig. 8.2 Step-by-step analysis of S parameters

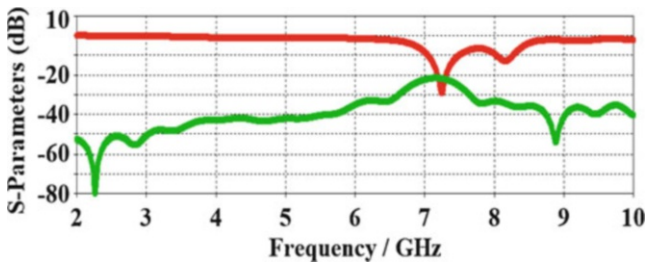


Fig. 8.3 S parameter comparison

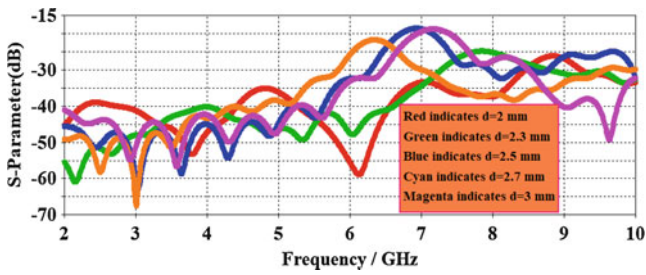
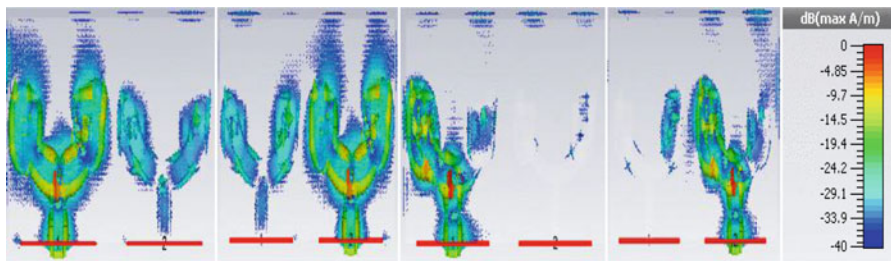


Fig. 8.4 S₂₁ Graph at different spacing between antennas



a) Port 1 excited 7.2 GHz b) Port 2 excited 7.2 GHz c) Port 1 excited 8.1 GHz d) Port 2 excited 8.1 GHz

Fig. 8.5 Surface current distribution of the design

the distribution of surface current vectors at 7.2 GHz as well as at 8.1 GHz. Figure 8.5a perceived that port #1 is excited and port #2 is terminated with a characteristic impedance of 50Ω load. In this case we observed that the maximum current flows through half-ring structure and observed that within a half ring a semi-circle is added with a square patch maximum current flowing. Figure 8.5b perceived that port #2 is excited and port #1 is terminated with 50Ω load observed that half-ring MIMO structure at bottom of the ring structure patch maximum current is flowing. For both the ports, the analogous distribution of surface current perceived that two homogenous elements were positioned side by side which can lead to create first resonant mode at 7.2 GHz. Similarly, the second resonant mode is at 8.1 GHz. Figure 8.5c shows the distribution of surface current vectors, maximum current flows at the left side of the half-ring resonator and a partial current flows through the edge of the microstrip connector and a little amount of current is observed at the left side of the half-ring patch. Figure 8.5d identified that maximum current flows through the left-side patch, a partial current is observed at the edge of the strip and a minimum surface current on right-side patch having a half-ring added to the square patch.

8.3 Results Analysis and Discussion

The simulated representation of S parameters satisfies the condition at dual band of operations of $|S_{11}| < -10$ dB and $|S_{11}| < -20$ dB. These parameters indicate that the proposed structure has a greater improvement in the parameters of transmission coefficient as well as reflection coefficients at the dual-band resonant frequencies of 7.2 and 8.1 GHz for the applications of C-band and X-band. Figure 8.6 shows the real/imaginary part of impedance verses frequency from 2.0 to 10 GHz. Figure 8.7 indicates the co- and cross-polarization effects with respect to the xz and yz planes having a dual-band operation at 7.2 and 8.1 GHz when one port of the antenna is excited and another port of the system is terminated with characteristic impedance of

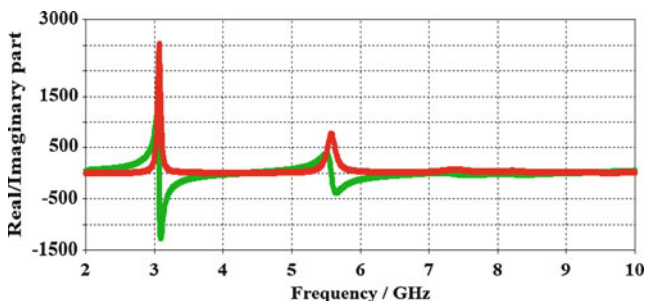


Fig. 8.6 Real/imaginary impedances

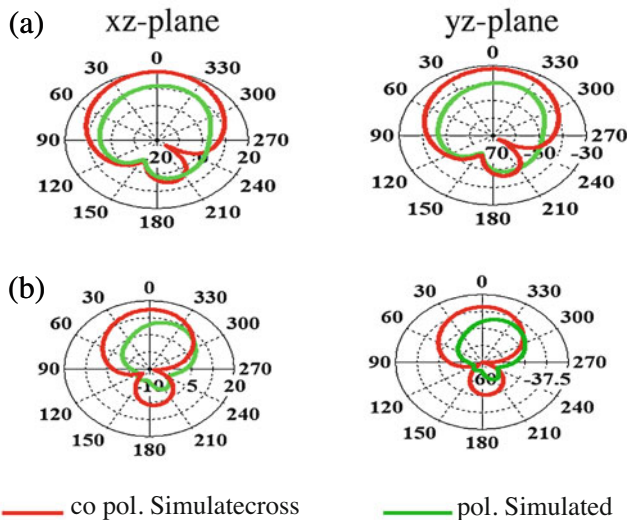


Fig. 8.7 Radiation patterns at dual-band (a) $f_1 = 7.2$ GHz and (b) $f_2 = 8.1$ GHz

50 Ω . It is observed that the pattern of radiation in xz plane is approximately analogous to pattern in the yz plane. It is important to identify that co-pol patterns are omnidirectional in nature in xz plane. Similarly, it is also to identify that the cross-pol component magnitude increases as the response of the frequency increases with horizontal direction component. Here, we observed that the co-pol is always outer region of the radiation pattern and cross-pol is inner side of the co-pol is a reasonably good agreement. Therefore, it can say that in order to placing half-ring antennas placing linearly the radiation patterns of separate elements lies on surface of a plane similar to each other by properly choosing the separation between the two radiating patches. It is also realized that the proposed structure helps to reduce the factor of mutual coupling.

Figure 8.8 shows the realized gain variations of the half-ring structure produced dual-band operation when port #1 is excited and port #2 is terminated with a 50 Ω load. When port #1 is excited, peak gain in first resonant band is 6 dBi and at another band is 4.8 dBi. Figure 8.9 shows the parameter of ECC which is lower than the 0.03. In time-domain analysis process group delay is a major important parameter. It shows how much time is considered for antenna to receive a pulse. There is a variation in group delay when placing the antenna front to front and side by side for 1 n. It validates the linear phase over entire far-field region. Figure 8.10 indicates the simulated result of group delay of 7.85 ± 1 n, -0.98 ± 1 ns over a resonant band of frequencies at 7.2 and 8.1 GHz. From the graph it is interesting to observe that the factor of negative group delay (NGD) increases, the signal attenuation increases and the bandwidth decreases.

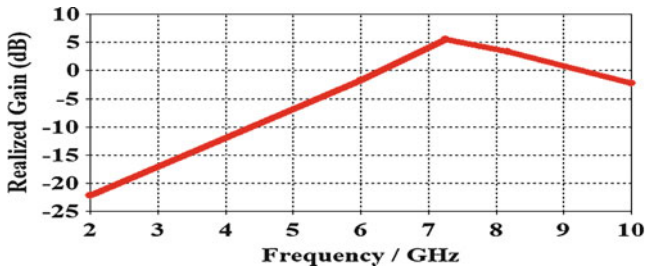


Fig. 8.8 Comparison of realized gain

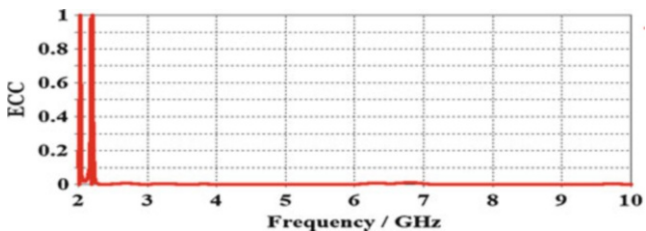


Fig. 8.9 ECC Simulation at 2.5 and 6.4 GHz

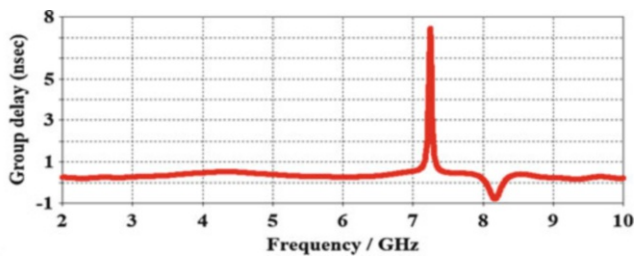


Fig. 8.10 Group delay of proposed design

8.4 Conclusion

A half-ring MIMO antenna, which consists of semi-half-ring added to a square patch, has been produced with dual-band characteristics at 7.2 and 8.1 GHz for C-band and X-band applications, respectively. The ineluctable suppression of the isolation has been attained by selecting the distance between the patches nearly $0.25 \lambda_0$. We observed that from the simulation results for the dual-band region $|S_{11}| < -10$ dB has been achieved and impedance matching maintained at $|S_{21}| < -20$ dB in the dual resonant frequencies. The group delays (GD) at the dual-band frequencies are 7.85 ± 1 ns and -0.98 ± 1 ns, and ECC value lower than

the 0.03 has been identified for the half-ring design. Thus, this system arrangement improves the parameter of antenna and good radiation patterns have been observed.

References

1. Irene G, Rajesh A (2018) A dual-polarized UWB–MIMO antenna with IEEE 802.11ac band-notched characteristics using split-ring resonator. *J Comp Electron*. <https://doi.org/10.1007/s10825-018-1213-x>
2. Liu YY, Tu ZH (2017) Compact differential band-notched UWB-MIMO antenna with common-mode suppression. *IEEE Antennas Wirel Propag Lett* 16:593–596
3. Babu KV, Anuradha B (2018) Design of multi-band Minkowski MIMO antenna to reduce the mutual coupling. *J King Saud Univ Eng Sci* 35:1–7
4. Braaten BD, Khan MS, Ijaz B, Capobianco AD, Naqvi A, Asif S (2015) Planar, compact ultra-wideband polarization diversity antenna array. *IET Microw Antennas Propag* 9:1761–1768
5. Chen LS, Lin GS, Sung H, Houng MP (2017) Isolation improvement in UWB MIMO antenna system using carbon black film. *IEEE Antennas Wirel Propag Lett* 16:222–225
6. Najam AI, Khan MS, Capobianco AD, Shafique MF, Shoaib I, Autizi E (2014) Compact ultra-wideband diversity antenna with a floating parasitic digitated decoupling structure. *IET Microw Antennas Propag* 8:747–753
7. Koul SK, Sipal D, Abegaonkar MP (2017) Easily extendable compact planar UWB MIMO antenna array. *IEEE Antennas Wirel Propag Lett* 16:2328–2331
8. Ryu KB, Lee JM, Kim HK, Woo JM (2012) A compact ultra wideband MIMO antenna with WLAN band-rejected operation for mobile devices. *IEEE Antennas Wirel Propag Lett* 11:990–993
9. Babu KV, Anuradha B (2018) Tri-band MIMO antenna for WLAN, WiMAX and defence system & Radio astronomy applications. *Adv Electromagn* 7:60–67
10. Toktas A (2016) G-shaped band-notched ultra-wideband MIMO antenna system for mobile terminals. *IET Microw Antennas Propag* 11(5):718–725